values showed a smaller change in T_2 with temperature change. This finding suggests that lower values of T_2 reflect a smaller scale of molecular motion, with lower activation energies.

Spin–lattice relaxation time (T_1) is known to reflect molecular mobility, similarly to T_2, but increases with decreasing T_2 (with decreasing molecular mobility) in the slow motional regime. The T_1 values of water protons in the presence of drug protons cannot be determined due to spin diffusion, but an approximate determination of T_1 for water protons is possible if the proportion of water protons is large. For example, in $Na_2HPO_4 \cdot 12H_2O$ and $Na_2HPO_4 \cdot 2H_2O$, water protons are predominant (24/25 and 4/5, respectively). $Na_2HPO_4 \cdot 12H_2O$ exhibits slower spin–spin relaxation (larger T_2) (Fig. 12), and faster spin–lattice relaxation (smaller T_1) (Fig. 13) compared to $Na_2HPO_4 \cdot 2H_2O$, which indicates that both T_1 and T_2 reflect the molecular mobility of hydration water. For the antibiotic hydrates examined, however, correlations between T_1 and T_2 were not observed, as shown in Figure 14. This finding indicates that for API hydrates containing a significant amount of drug protons, such as antibiotic hydrates, the molecular mobility of the hydration water is not reflected in T_1.

Hydration Water Showing Gaussian Decay

As mentioned previously, all of the API hydrates other than the four antibiotic hydrates exhibited only Gaussian decay (Fig. 2). The value of T_2 did not vary significantly among the API hydrates, as shown in Figure 15. Furthermore, the onset temperatures of the single endothermic peaks

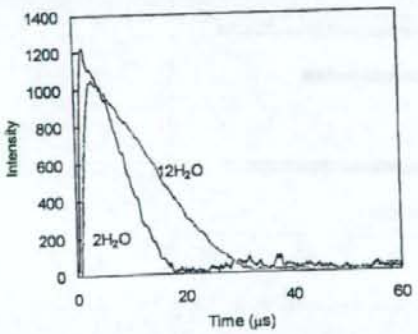

Figure 12. Free induction decay for Na_2HPO_4 $12H_2O$ and $2H_2O$.

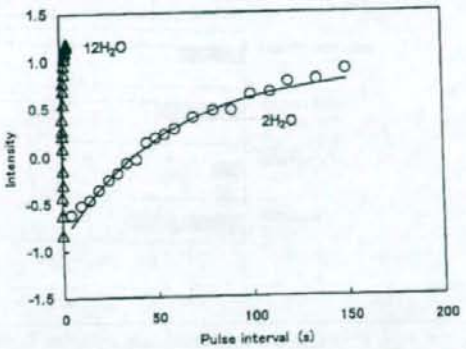

Figure 13. Spin–lattice relaxation for Na_2HPO_4 $12H_2O$ and $2H_2O$.

due to water evaporation for quinidine sulfate, pipemidic acid, and sulpyrine hydrates (Fig. 5), as well as each of the two peaks due to water evaporation observed for quinine hydrochloride, scopolamine hydrobromide, saccharin sodium, and berberine chloride hydrates (Fig. 4), were not correlated with T_2. These findings indicate that the molecular mobility of hydration water that shows Gaussian decay is too low to be reflected in T_2. No correlation between T_2 and molecular mobility is supported by the finding that changes in T_2 associated with changes in temperature were much smaller than those observed for the antibiotic hydrates that exhibited Lorentzian decay, as exemplified by pipemidic acid (Fig. 10). Such low molecular mobility may be attributed to water molecules firmly trapped in the crystal lattice, rather than water molecules trapped in voids in the crystal.

For quinidine sulfate, pipemidic acid, and sulpyrine hydrates, a single endothermic peak was observed in DSC (Fig. 5). The water content versus humidity plots showed a flat line at a certain number of water molecules. Pipemidic acid and sulpyrine showed a flat line at three and one water molecule(s) per hydrate, respectively, and evaporation of these water molecules was observed only under very low humidity (Fig. 7). These findings indicate that water molecules are firmly trapped in the crystal.

For quinine hydrochloride, scopolamine hydrobromide, saccharin sodium, and berberine chloride hydrates, two endothermic peaks were shown in DSC (Fig. 4). The water content versus humidity plots for these hydrates (except for berberine chloride) showed flat lines at two levels

DOI 10.1002/jps

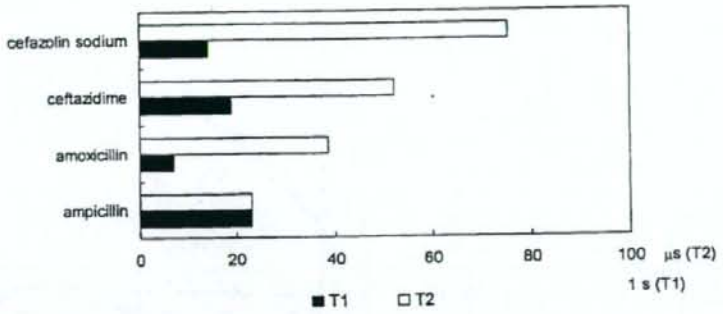

Figure 14. Correlation between T_1 and T_2 for four antibiotic hydrates.

of water content (Fig. 8), suggesting the presence of two water populations: molecules that evaporate at high humidity, and others that evaporate at lower humidity (below 10% RH). This seems to be consistent with the observation of two endothermic peaks in DSC. The endothermic peak observed at a high temperature and the flat line observed at a low humidity may be attributable to hydration water with strong hydrogen–bonding interactions, while the one observed at a lower temperature and higher humidity may be attributable to hydration water with week interactions. The presence of hydration water with week interactions is also supported by the finding that the water contents as measured by the Karl Fischer method were smaller than those specified in the JP (Tab. 1).

CONCLUSION

It was found that spin–spin relaxation time, T_2, is a useful parameter that can indicate the molecular mobility of water of hydration which has relatively high mobility and shows Lorentzian decay upon spin–spin relaxation. For these water molecules, molecular mobility as determined by T_2 is correlated with ease of evaporation both under nonisothermal and isothermal conditions,

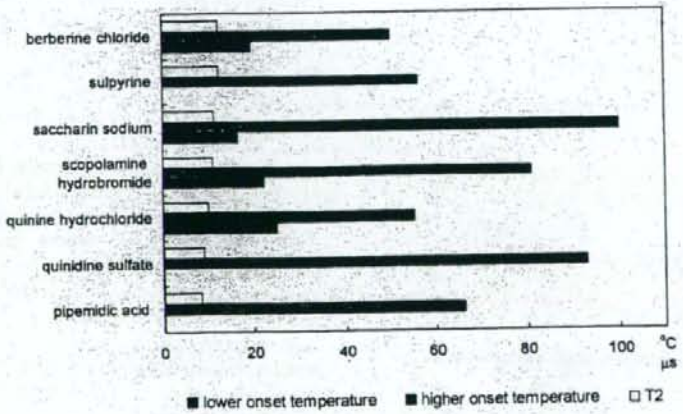

Figure 15. Correlation between onset temperature and T_2 for API hydrates that show Gaussian decay.

such that water molecules with greater ease of evaporation have higher T_2 values.

In contrast, for hydration water that has low mobility and shows Gaussian decay, T_2 was found not to correlate with ease of evaporation under nonisothermal conditions, suggesting that molecular motion that determines the ease of evaporation is not reflected in T_2; in this case, T_2 cannot be used as a parameter to indicate molecular mobility.

The water molecules in the API hydrates studied were found to have wide-ranging molecular mobilities, from low molecular mobility that could not be evaluated by NMR relaxation times, such as the water molecules in pipemidic acid hydrate, to high molecular mobility that could be evaluated by NMR relaxation times, such as the water molecules in ceftazidime hydrate.

REFERENCES

1. Yoshioka S, Aso Y. 2007. Correlations between molecular mobility and chemical stability during storage of amorphous pharmaceuticals. J Pharm Sci 96:960–981.
2. Ahlneck C, Zografi G. 1990. The molecular basis for moisture effects on the physical and chemical stabiity of drugs in the solid state. Int J Pharm 62:87–95.
3. Mimura H, Gato K, Kitamura S, Kitagawa T, Kohda S. 2002. Effect of water content on the solid-state stability in two isomorphic clathrates of cephalosporin: Cefazolin sodium pentahydrte (α form) and KF041 hydrate. Chem Pharm Bull 50: 766–770.
4. Zografi G. 1988. States of water associated with solids. Drug Dev Ind Pharm 14:1905–1926.
5. Newman AW, Reutzel-Edens SM, Zografi G. 2007. Characterization of the "hygroscopic" properties of active pharmaceutical ingredients. J Pharm Sci DOI: 10.1002/jps.21033.
6. Brittain HG, Grant DJW. 1999. Effect of polymorphism and solid state solvation on solubility and dissolution rate. In: Brittain HG, editor. Polymorphism in pharmaceutical solids. New York: Marcel Dekker. pp 279–330.
7. Shinyashiki N, Asaka N, Mashimo S. 1990. Dielectric study on dynamics of water in polymer matrix using a frequency range 10^6–10^{10} Hz. J Chem Phys 93:760–764.
8. Ahlqvist MU, Taylor LS. 2002. Water dynamics in channel hydrates investigated using H/D exchange. Int J Pharm 241:253–261.
9. Ruan R, Chen PL. 1998. Mobility of water in food and biological systems. In: Water in foods and biological materials, a nuclear magnetic resonance approach. Lancaster, PA: Technomic Publishing Company, Inc. pp 149–228.
10. Oksanen CA, Zografi G. 1993. Molecular mobility in mixtures of absorbed water and solid poly(vinylpyrrolidone). Pharm Res 10:791–799.
11. Otsuka T, Yoshioka S, Aso Y, Kojima S. 1995. Water mobility in aqueous solutions of macromolecular pharmaceutical excipients measured by oxygen-17 nuclear magnetic resonance. Chem Pharm Bull 43:1221–1223.
12. Mansfield P. 1965. Multiple-pulse nuclear magnetic resonance transients in solids. Phys Rev 137:A961–A974.
13. Parizel N, Meyer G, Weill G. 1993. Nuclear magnetic resonance linesahape studies of interpenetrating polymer networks. Polymer 12:2495–2502.
14. Morris KR. 1999. Structural aspects of hydrates and solvates. In: Brittain HG, editor. Polymorphism in pharmaceutical solids. New York: Marcel Dekker. pp 125–181.

DOI 10.1002/jps

J Pharmacol Sci 107, 285 – 294 (2008)

Journal of Pharmacological Sciences

Full Paper

The Novel Compounds That Activate Farnesoid X Receptor: the Diversity of Their Effects on Gene Expression

Takuo Suzuki[1,2,*], Norimasa Tamehiro[3], Yoji Sato[4], Tetsu Kobayashi[1], Akiko Ishii-Watabe[1], Youichi Shinozaki[5], Tomoko Nishimaki-Mogami[3], Toshihiro Hashimoto[6], Yoshinori Asakawa[6], Kazuhide Inoue[7], Yasuo Ohno[5], Teruhide Yamaguchi[1], and Toru Kawanishi[1]

[1]*Division of Biological Chemistry and Biologicals,* [3]*Division of Biosignaling,* [4]*Division of Cellular and Gene Therapy Products,* [5]*Division of Pharmacology, National Institute of Health Sciences, Tokyo 158-8501, Japan*
[2]*Pharmaceuticals and Medical Device Agency, Tokyo 100-0013, Japan*
[6]*Faculty of Pharmaceutical Sciences, Tokushima Bunri University, Tokushima 770-8514, Japan*
[7]*Graduate School of Pharmaceutical Sciences, Kyushu University, Fukuoka 812-8582, Japan*

Received January 8, 2008; Accepted May 16, 2008

Abstract. Farnesoid X receptor (FXR) controls the expression of critical genes in bile acid and cholesterol homeostasis. To study FXR and to develop a regulator of cholesterol, some non-steroidal and steroidal ligands have been found in addition to endogenous ligands for FXR. In this study, we discovered five bile acid derivatives (methyl cholate, methyl deoxycholate, 5β-cholanic acid, 5β-cholanic acid-7α,12α-diol, and NIHS700) and two natural products (marchantin A and marchantin E) that activated FXR in the reporter assay. These compounds activated FXR to a high level comparable to the most potent endogenous bile acid, chenodeoxycholic acid, although it was not predicted from their structures; five of them were similar to the lower potency bile acids, and two were structurally much different from bile acids. The elevation levels of reporter gene expression by some of the screened compounds were varied in Cos-7, HepG2, HuH-7, and Caco-2 cells. These compounds also controlled the expression of genes regulated by FXR, and some of the compounds regulated these genes in a cell-type–specific and/or gene-selective fashion. Therefore, molecular design of the compounds can cause selective modulation of the expression of FXR target genes.

Keywords: farnesoid X receptor (FXR), reporter assay, ginkgolic acid, marchantin, cell-type–specific modulation

Introduction

The farnesoid X receptor (FXR, *NR1H4*) is a member of the nuclear-receptor superfamily. Nuclear receptors are ligand-activated transcription factors that are involved in a variety of physiological, developmental, and toxicological processes. The nuclear-receptor superfamily includes receptors for thyroid and steroid hormones, retinoids, and vitamin D, as well as receptors for unknown ligands. These receptors share a highly conserved DNA-binding domain and a discrete ligand-binding domain; and they bind to hormone response elements (HRE) on the DNA during the formation of homodimers, heterodimers, or monomers. The ligand-binding to nuclear receptors leads to a conformational change of these receptors and the recruitment of coactivator complexes, resulting in transcriptional activation (1). Their ligand-dependent activity makes nuclear receptors good pharmacological targets.

FXR is a receptor for bile acids such as chenodeoxycholic acid (CDCA), deoxycholic acid, cholic acid, and their conjugates. Bile acids are synthesized in the liver and secreted into the intestine, where their physical properties facilitate the absorption of fats and vitamins through micelle formation. Cholesterol disposal from the liver is also dependent on the bile acid composition of the secreted bile. FXR is activated by bile acids and controls the expression of critical genes in bile

*Corresponding author (affiliation #1). tsuzuki@nihs.go.jp
Published online in J-STAGE on July 5, 2008 (in advance)
doi: 10.1254/jphs.08006FP

acid and cholesterol homeostasis such as the bile salt export pump (*BSEP*), small heterodimer partner (*SHP*), *CYP7A1*, ileal bile acid-binding protein (*IBABP*), and phospholipid transfer protein (*PLTP*) (2 – 4). FXR plays a critical role in lipid metabolism since FXR-null mice showed elevated serum cholesterol and triglyceride levels (5), and an FXR agonist has been shown to reduce serum triglyceride levels (6). Moreover, an FXR agonist has been reported to confer hepato-protection in a rat model of cholestasis (7). Recently, FXR has also been reported to mediate glucose metabolism and to protect the intestinal mucosa from bacterial overgrowth and inflammatory insults (8, 9). Therefore, the development of FXR agonists might prove useful for the treatment of a wide variety of diseases, including diabetes, cholesterol gallstones, and hepatic and intestinal toxicity.

In addition to bile acids, some compounds whose structures are much different from bile acids (e.g., GW4064) and several selective modulators (e.g., guggulsterone and AGN34) that regulate a subset of FXR-specific genes have been identified as FXR ligands (10, 11). These compounds other than bile acids are useful for analysis of the role of FXR in lipid and glucose metabolism because they may not have the FXR-independent property of bile acids (e.g., dietary lipid absorption) and are not metabolized to form harmful lithocholic acid. On the other hand, selective ligands have been studied in detail regarding the other nuclear receptors (e.g., selective estrogen-receptor modulators (SERMs)). These compounds exhibit variable effects (e.g., function as agonists or antagonists) depending on the cells and tissues, and they have been used in therapy (e.g., tamoxifen and raloxifen). Because FXR has been found to play many roles in addition to lipid metabolism, selective FXR modulators might be useful for therapy.

We previously reported the reporter assay system of FXR, RAR, and RXR using green fluorescent protein derivatives (12). We screened a compound library (NIHS library containing about 700 compounds) and found five bile acid derivatives (methyl cholate, methyl deoxycholate, 5β-cholanic acid, 5β-cholanic acid-7α,12α-diol, and NIHS700) and two natural products (marchantin A and marchantin E) as FXR activators. Concerning these seven compounds and ginkgolic acids that we previously showed as FXR activators, we investigated the FXR activation by reporter assay in four types of cells and the expression of the genes regulated by FXR. These compounds activated FXR comparably to the most potent bile acid, and some controlled the expression of genes regulated by FXR in a cell-type–specific and/or gene-selective fashion.

Materials and Methods

Chemicals

Methyl cholate, methyl deoxycholate, 5β-cholanic acid, and 5β-cholanic acid-7α,12α-diol were purchased from Steraloids, Inc. (Newport, RI, USA). NIHS700 was provided from Research Foundation Itsuu Laboratory (Tokyo). Ginkgolic acid 15:1 was purified *Ginkgo biloba L.* var. *diptera* as described previously (12). Ginkgolic acid 17:1 was purchased from Nagara Science (Gifu). Chenodeoxycholic acid was purchased from Sigma-Aldrich (St. Louis, MO, USA). Cholic acid, deoxycholic acid and lithocholic acid were purchased form Wako (Osaka).

Isolation of marchantins A and E from Marchantia paleacea var. diptera

Fresh material (6.67 kg) of *Marchantia paleacea* var. *diptera* collected in Tokushima, Japan in 1993 was extracted with MeOH (10 L) for 1 month at room temperature. The extract was filtered and evaporated *in vacuo* to afford a brown residue (176.0 g), which was subjected repeatedly to column chromatography (CC) on silica gel (*n*-hexane-EtOAc, gradient) and Sephadex-LH-20 ($CHCl_3$-MeOH = 1:1) to afford marchantin A (79.5 g) and marchantin E (8.34 g) (13, 14).

Plasmid construction

The construction of plasmids for the reporter assay using green fluorescent protein (GFP) derivatives has been described in a previous report (12). For expression of FXR and RXRα, the ORF region of human FXR or human RXRα (accession number U68233, X52773) was inserted into pcDNA3.1 (Invitrogen, Carlsbad, CA, USA). For reporter plasmids, the FXR response element (4 copies of DR1: ggatccaaactgaGGGTCAgTGACCC aagtgaaaaactgaGGGTCAgTGACCCaagtgagaattcaaact gagGGTCAgTGACCCaagtgaaaaactgaGGGTCAgTGA CCCaagtgaagatct), the 3' region (201 bp) of cytomegalovirus (CMV201) promoter, and enhanced yellow fluorescent protein (EYFP) were ligated. As an internal control plasmid, the luciferase gene of pGL3-Control Vector (Promega, Madison, WI, USA) was replaced with enhanced cyan fluorescent protein (ECFP).

For a reporter assay using luciferase, FXRE was inserted into the *Mlu*I and *Bgl*II sites of pGL3-Control Vector, and the SV40 promoter was replaced with minimal CMV promoter. The phRL-CMV vector (Promega) was used as an internal control vector.

The reporter assay using GFP derivatives

A monkey kidney cell line, COS-7, was kept in DMEM (Sigma-Aldrich) with penicillin (100 unit/ml),

streptomycin (100 μg/ml), and 10% FBS. Transfections were performed using Effectene transfection reagent (Qiagen, Valencia, CA, USA) according to the manufacturer's instructions. The ratio of the reporter plasmid, FXR expression plasmid, RXR expression plasmid, and the internal control plasmid was 4:1:1:1. The culture medium was replaced with DMEM without phenol red (GIBCO, Carlsbad, CA, USA) supplemented with 10% charcoal-treated FBS (Hyclone, Logan, UT, USA) when the transfections were performed. At 15 h after transfection, the cells were treated with trypsin-EDTA (GIBCO) and divided among wells of a black 96-well plate with 100 μl of the culture medium. At 6 h after division among wells, the cells were treated with chemicals. After 40-h incubation, the medium was eliminated by decantation, the cells were washed twice with PBS, and the wells were filled with 200 μl PBS. Fluorescence was detected using a microplate reader (ARVO; Perkin Elmer, Fremont, CA, USA). The fluorescence of EYFP was detected with an excitation filter of 485 nm and an emission filter of 545 nm, and that of ECFP was detected with filters of 420 nm and 486 nm (Perkin Elmer), respectively. The autofluorescence in COS-7 cells was subtracted from each of the detected fluorescences, and the EYFP/ECFP ratio was calculated using the resulting values.

The reporter assay using luciferase

The human hepatocyte cell line HepG2 was kept in MEM (Sigma-Aldrich) with penicillin (100 unit/ml), streptomycin (100 μg/ml), and 10% FBS. The cells were transfected with 3 times more plasmids than recommended with salmon sperm DNA (200 ng for 1 well of a 6-well plate) using Effectene transfection reagent (Qiagen). In contrast, the human hepatocyte cell line HuH-7 was kept in DMEM with penicillin (100 unit /ml), streptomycin (100 μg/ml), and 10% FBS; and the human intestinal cell line Caco-2 was kept in DMEM with penicillin (100 unit/ml), streptomycin (100 μg /ml), 10% FBS, and 100 μM MEM Non-Essential Amino Acids Solution (GIBCO). HuH-7 and Caco-2 cells were transfected with plasmids using Effectene transfection reagent (Qiagen) according to the manufacturer's instructions. The ratio of the reporter plasmid using luciferase, the FXR expression plasmid, RXR expression plasmid, and the internal control plasmid using *renilla* luciferase was 4:1:1:1. FBS of the culture medium was replaced with charcoal-treated FBS (Hyclone) when the transfections were performed. The following manipulations were the same as those used in the reporter assay with GFP derivatives. After 40-h treatment with the compounds, measurement of luciferase and *renilla* luciferase was performed with the Dual-Glo™ Luciferase Assay System (Promega) according to the manufacturer's instructions.

TaqMan primers and probes

Oligonucleotide primers and probes for human *BSEP*, *SHP*, and *CYP7A1* were synthesized by Applied Biosystems (Foster City, CA, USA). These sequences (5' to 3') were as follows: Human *BSEP*, forward primer (GGGCCATTGTACGAGATCCTAA), probe (6FAM-TCTTGCTACTAGATGAAGCCACTTCTGCCTTAGA-TAMRA) and reverse primer (TGCACCGTCTTTT CACTTTCTG); Human *SHP*, forward primer (GGTG CAGTGGCTTCAATGC), probe (6FAM-TCTGGAG CCTGGAGCTTAGCCCCA-TAMRA), and reverse primer (GGTTGAAGAGGATGGTCCCTTT); Human *CYP7A1*, forward primer (GAGAAGGCAAACGGGT-GAAC), probe (6FAM-TGGATTAATTCCATACCTG GGCTGTGCTCT-TAMRA), and reverse primer (GGT ATGACAAGGGATTTGTGATGA). The primers and probe for 18S rRNA were also purchased from Applied Biosystems.

RNA isolation and real-time quantitative PCR

The culture medium of HepG2, HuH-7, and Caco-2 cells was replaced with the medium supplemented with 10% charcoal-treated FBS (Hyclone) at 24 h before treatment with the compounds. The cells were treated with the tested chemicals for 24 h, and total RNA was then prepared using the RNeasy purification system according to the manufacturer's instructions (Qiagen). Reverse transcription reactions and TaqMan-PCRs were performed using the High-Capacity cDNA Archive Kit (Applied Biosystems) and the TaqMan Universal PCR Master Mix (Applied Biosystems) according to the manufacturer's instructions. Sequence-specific amplification was quantified with the ABI Prism 7700 sequence detection system (Applied Biosystems), and values were normalized to 18S rRNA.

Results

We found seven compounds that activate FXR (the chemical structures of which are shown in Fig. 1A) using the reporter assay system described by Suzuki et al. (12). In the reporter assay system, two fluorescent proteins, EYFP and ECFP, were used for detection of FXR activation and as an internal control, respectively. The activation of FXR by the seven compounds and some endogenous ligands [i.e., cholic acid (CA), deoxycholic acid (DCA), lithocholic acid (LCA), and chenodeoxycholic acid (CDCA)] is shown as the increased ratio of EYFP/ECFP fluorescence intensity in the upper panel of Fig. 2A. As a control, the reporter vector

A

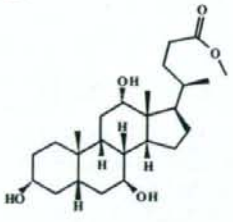

Methyl cholate

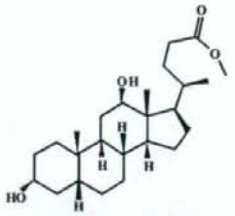

Methyl deoxycholate

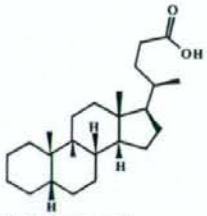

5β-cholanic acid

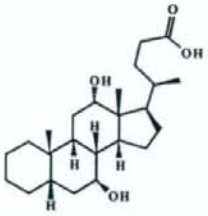

5β-cholanic acid 7α,12α-diol

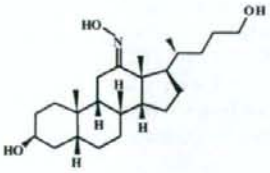

NIHS 700

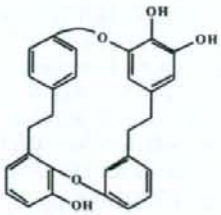

Marchantin A

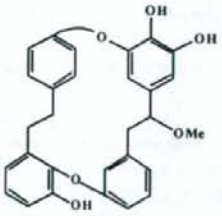

Marchantin E

B

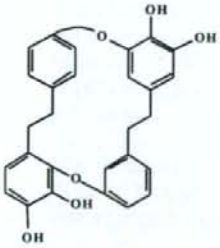

Marchantin B

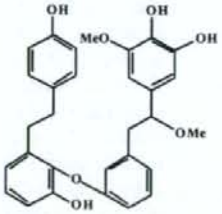

Paleatin B

C

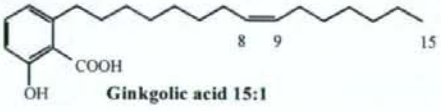

Ginkgolic acid 15:1

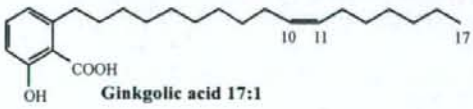

Ginkgolic acid 17:1

Fig. 1. Structure of the compounds that activated FXR and their related compounds. A: Structure of the compounds that activated FXR as determined by the reporter assay. B: The compounds similar to marchantin A and marchantin E. C: Ginkgolic acid 15:1 and ginkgolic acid 17:1 that highly activated FXR described in Ref. 12.

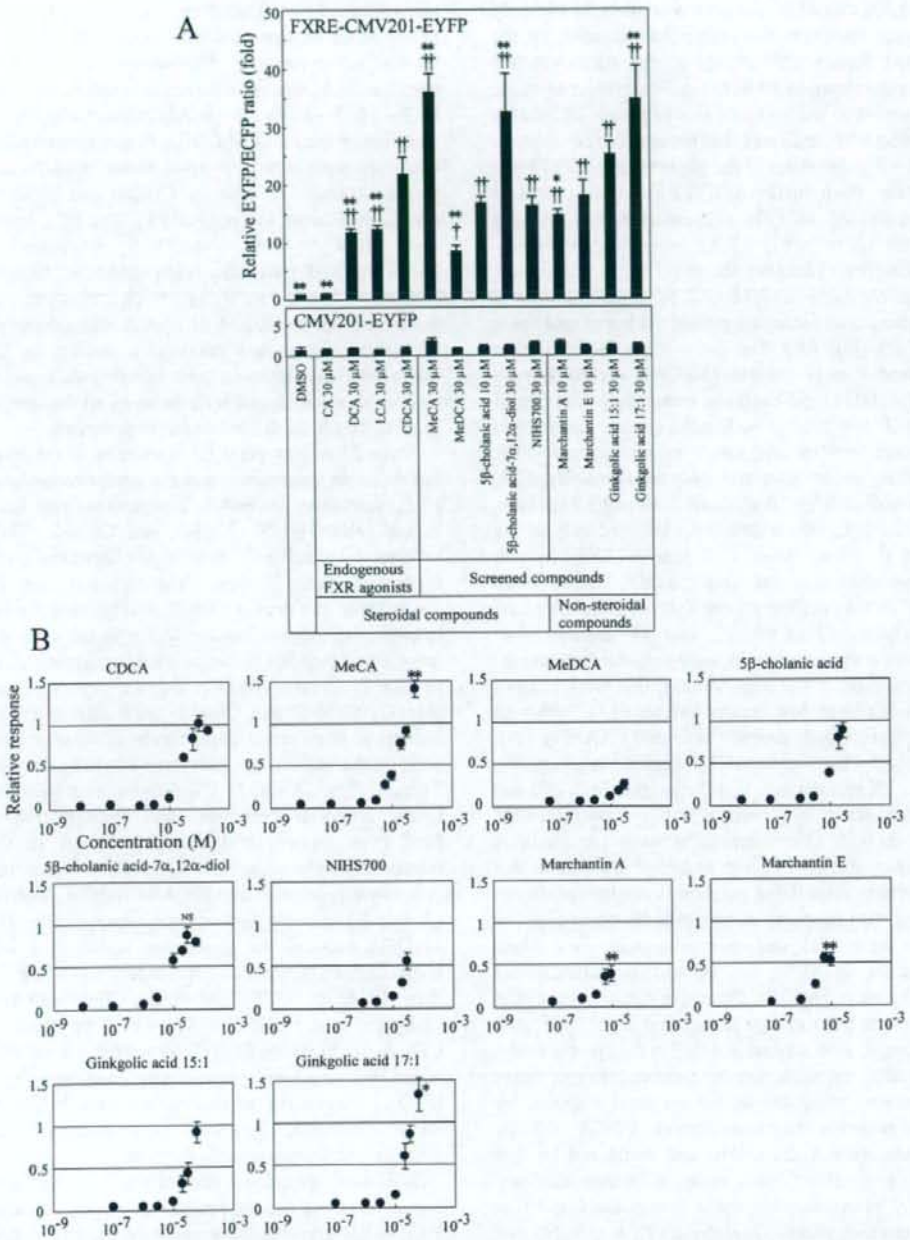

Fig. 2. Response in the reporter expression. A: The activation of FXR. COS-7 cells were transfected with the reporter plasmid containing FXRE, the expression plasmids of FXR and RXRα, and the internal control plasmid. The transfected cells were treated with each compound. All values are means ± S.D., n = 4. $^{\dagger}P<0.05$ *vs* DMSO, $^{\dagger\dagger}P<0.01$ *vs* DMSO, $^{*}P<0.05$ *vs* CDCA (30 μM), $^{**}P<0.01$ *vs* CDCA (30 μM), according to Dunnett's test. B: Dose–response analyses on the reporter assay of FXR. The response was shown as a ratio, compared with that by CDCA at 100 μM. All values are means ± S.D., n = 4. $^{*}P<0.05$, $^{**}P<0.01$; NS, not a significant difference, compared with CDCA at 100 μM according to Student's *t*-test.

without FXR response element was used in place of the reporter vector to determine the response by the unexpected factors (the change in the transcriptional efficiency unrelated to FXR, the self-fluorescence of the tested chemicals, and so forth) (lower panel of Fig. 2A). Moreover, it was confirmed that these seven compounds activated the expression of the reporter gene EYFP via FXR because the induction of EYFP expression required cotransfection of an FXR expression vector and the compounds did not activate RXR homodimer and RAR-RXR heterodimer (data not shown).

The seven compounds could be separated into 2 groups: those that contained steroid skeletons and those that did not (Fig. 1A). The compounds in the former group were methyl cholate (MeCA), methyl deoxycholate (MeDCA), 5β-cholanic acid, 5β-cholanic acid-7α,12α-diol, and NIHS700. Methyl cholate and methyl deoxycholate are methyl esters of endogenous FXR ligands (i.e., cholic acid and deoxycholic acid). FXR was also activated by 5β-cholanic acid and 5β-cholanic acid-7α,12α-diol, whose structures differed only in the 3α-hydroxyl group from endogenous FXR ligands (i.e., lithocholic acid and cholic acid). The structure of NIHS700 was different from that of lithocholic acid at the substituents of the 11- and 24-positions. The compounds in the latter group, non-steroidal compounds, were marchantin A and marchantin E that were isolated from the liverwort Marchantia species (13). Although these two compounds strongly activated FXR (Fig. 2A), marchantin B and paleatin B (shown in Fig. 1B), analogues of marchantin A and marchantin E, did not cause such activation, even at higher concentrations (data not shown). The difference between marchantin A and marchantin B is only one hydroxyl group, and that between marchantin E and paleatin B is ring-opening or not. Along with the seven compounds shown in Fig. 1A, ginkgolic acid 15:1 and ginkgolic acid 17:1 (their structures are shown in Fig. 1C and the activation of FXR is shown in Fig. 2A), the major constituents of the crude extracts from ginkgo leaves that highly activated FXR (12) were also studied in detail in the present study.

In Fig. 2B, we show the dose-dependency of these compounds as compared to the maximal response by the most potent endogenous ligand, CDCA. All the compounds were hydrophobic and could not be dissolved at over 30 – 60 μM, each, in culture medium. Moreover, responses by some compounds even at soluble concentrations (Marchantin E at 30 μM and MeDCA at 60 μM) could not be measured due to their toxicity. Therefore, we could not obtain the data at higher concentrations. Although the value of treatment with 30 μM 5β-cholanic acid is shown in Fig. 2B, this compound slightly separated out from the solution at this concentration. Therefore, the concentration applied in the other experiments was limited to 10 μM. Since the EC_{50} values of 5β-cholanic acid-7α,12α-diol, marchantin A, and marchantin E could be estimated to be 3 – 10, 3 – 6, and 3 – 6 μM, respectively, the values were lower than that of CDCA (approximately 30 μM). Maximal activation by 5β-cholanic acid-7α,12α-diol was comparable to that by CDCA, but those by the marchantins were lower (P<0.01). The EC_{50} and maximal values of MeCA, MeDCA, 5β-cholanic acid, NIHS700, and ginkgolic acids could not be assessed because of low solubility or toxicity. However, activations of FXR by 60 μM of MeCA and ginkgolic acid 17:1 were higher than maximal activation by CDCA. Since the EC_{50} values of the 6 compounds could not be estimated, we analyzed activations by all the compounds at 30 or 10 μM in the following experiments.

Since FXR was primarily localized in the liver and intestine, we determined that the compounds also act as FXR activators in cultured hepatoma and intestinal cancer cells (HepG2, HuH-7, and Caco-2 cells). The reporter assay using GFP derivatives could be applied to these cell lines. However, the signal of the internal control was less than in COS-7 cells because the internal control plasmid was not replicated in the cells without large T antigen. We therefore used luciferase (LUC) and *renilla* luciferase (RLUC) for the reporter assay in HepG2, HuH-7, and Caco-2 cells. The extent of the induction with some compounds differed among the cells on the basis of the activation extent by endogenous ligands (Figs. 2A and 3). The differences are enumerated below. Reporter expression was strongly induced by MeCA to higher level than by CDCA in COS-7, moderately induced in HuH-7, and only weakly induced to a lower level than by CDCA in HepG2. Marchantins (A and E) scarcely induced the expression in HepG2. MeDCA induced the expression higher than LCA in HepG2 (P<0.05, according to Student's t-test), but lower than LCA in COS-7 (P<0.01). The induction by ginkgolic acid 17:1 in HepG2 was lower than that by CDCA, but higher in COS-7. Moreover, the induction by NIHS700 in Caco-2 was lower than that by LCA (P<0.05, according to Student's t-test), but higher in COS-7 (P<0.01). These compounds seemed to activate FXR in a cell-type–specific fashion.

We then examined the effects of the screened compounds on the expression of genes regulated by FXR. FXR controls the expression of critical genes in bile acid and cholesterol homeostasis (2 – 4). In this experiment, we detected the expression of three genes, bile salt export pump (*BSEP*), small heterodimer partner (*SHP*), and *CYP7A1*. By FXR activation, the expression of *BSEP* and *SHP* genes are directly upregulated, and

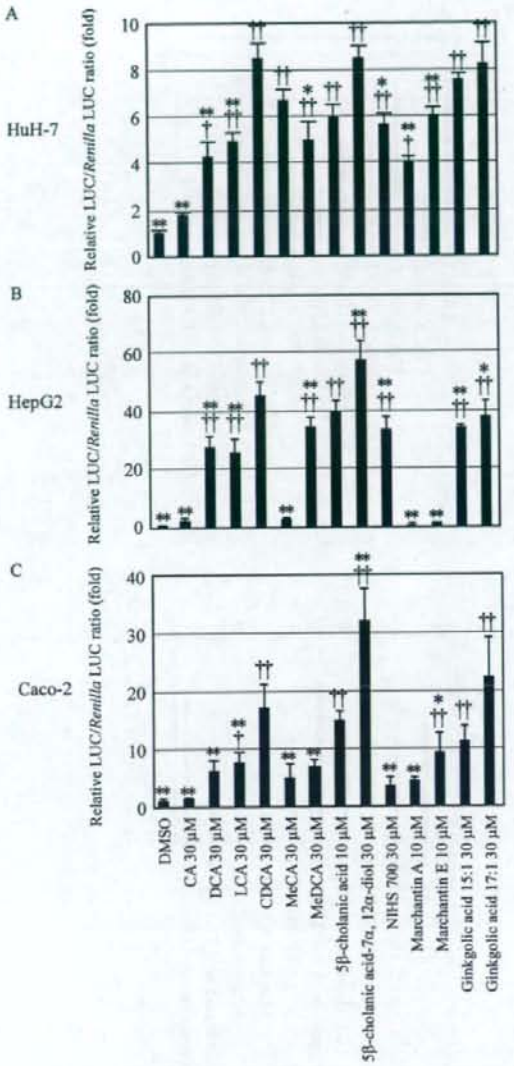

Fig. 3. The difference of FXR-activation in the reporter assay. A: The activation of FXR in HuH-7 cells is shown. HuH-7 cells were transfected with the reporter plasmid containing FXRE and luciferase, the expression plasmids of FXR and RXRα, and the internal control plasmid containing *renilla* luciferase. The transfected cells were treated with each compound. Data are shown as the means ± S.D. derived from four wells. $^{\dagger}P<0.05$ *vs* DMSO, $^{\dagger\dagger}P<0.01$ *vs* DMSO, $^{*}P<0.05$ *vs* CDCA (30 μM), $^{**}P<0.01$ *vs* CDCA (30 μM), according to Dunnett's test. The activation of FXR in HepG2 and Caco-2 cells is shown in the middle and lower panel, respectively. Except for the cell type, all manipulations were the same as those shown above. B: HepG2 cells, n = 4. C: Caco-2 cells, n = 4 – 5.

that of *CYP7A1* gene is indirectly down-regulated. HepG2 cells without transfection of artificial genes were treated with the compounds, and the amount of the mRNAs was measured by real-time quantitative PCR. The expression of the genes in HepG2 cells is shown in Fig. 4 (A – C). The compounds other than MeCA, 5β-cholanic acid, marchantin A, and marchantin E significantly induced the expression of *SHP* mRNA ($P<0.05$ *vs* DMSO, according to Dunnett's test). Because *BSEP* was expressed only at low levels in HepG2 cells, Fig. 4C showed scattered results. However, the change in *BSEP* expression was similar to the change in *SHP* expression. On the other hand, the reduction levels of *CYP7A1* mRNA by some compounds differed from the change of *SHP* mRNA levels. The reduction in *CYP7A1* mRNA accumulation by MeDCA was lower than that by CDCA, although the compound induced *SHP* mRNA accumulation to a higher level than CDCA. Moreover, marchantin A and E reduced *CYP7A1* mRNA accumulation ($P<0.05$ *vs* DMSO), although the regulation of *SHP* mRNA accumulation was not detected.

Moreover, regulation of gene expression in a cell-type–specific fashion was also detected (Fig. 4D). The induction of *BSEP* expression by MeCA in HuH-7 cells was higher than that of *BSEP* and *SHP* expression in HepG2 cells, and that by MeDCA was lower. These results indicate that the screened compounds could regulate the expression of critical genes in bile acid and cholesterol homeostasis and suggested that MeCA, MeDCA, marchantin A, and marchantin E possibly regulate expression of the genes in a cell-type–specific and/or gene-species selective fashion.

Discussion

In this paper, we found five steroidal compounds and two non-steroidal compounds that activate FXR. These compounds possess some properties that differ from those of CDCA.

First, two of the steroidal compounds, 5β-cholanic acid and 5β-cholanic acid-7α,12α-diol, were found to be effective ligands for FXR in a reporter assay and in quantitative real-time PCR. The crystal structure of the FXR ligand binding domain was analyzed as a complex with 3-deoxyCDCA and revealed that the 3-hydroxyl group was not responsible for the activation of FXR (15). However, FXR was activated to lower levels by lithocholic acid and cholic acid, whose structures were different only in the 3α-hydroxyl group from 5β-cholanic acid and 5β-cholanic acid-7α,12α-diol. In this case, elimination of the 3-hydroxyl group increased the potency of the activation.

The other three steroidal compounds were MeCA,

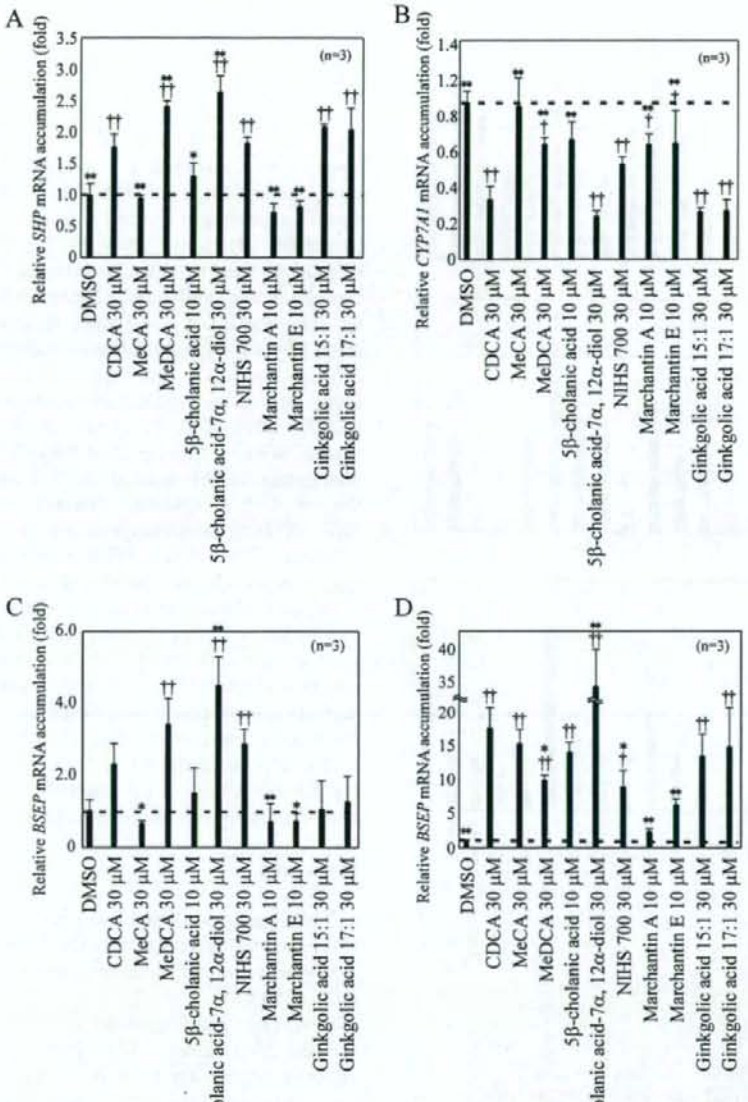

Fig. 4. Expression of *SHP*, *CYP7A1*, and *BSEP* genes in cells treated with the compounds. HepG2 cells were treated with each compound for 24 h. Accumulation of *SHP* (A), *CYP7A1* (B), and *BSEP* (C) mRNA in HepG2 cells was detected by real-time quantitative PCR. D: Accumulation of *BSEP* mRNA in HuH-7 cells treated with each compound for 24 h. All values are means ± S.D., n = 3. †$P<0.05$ *vs* DMSO, ††$P<0.01$ *vs* DMSO, *$P<0.05$ *vs* CDCA (30 μM), **$P<0.01$ *vs* CDCA (30 μM), according to Dunnett's test.

MeDCA, and NIHS700. Although the structures of these compounds were similar to those of the endogenous ligands, the slight modification of bile acids caused different regulation of FXR. It has been suggested that

the binding of bile acids with a slightly different structure (CA, DCA, UDCA, and CDCA) resulted in different FXR conformations, which in turn differentially regulated expression of individual FXR targets (16). Therefore, these compounds may also produce different FXR conformations than that produced by CDCA. In fact, MeDCA showed different properties in the regulation of the genes as compared to CDCA. DCA, CA, and UDCA have been reported to partially increase *BSEP* expression, but repress *CYP7A* mRNA with nearly equal effects as CDCA (16). Adversely, MeDCA strongly induced *BSEP* mRNA, but only weakly reduced *CYP7A1* mRNA (Fig. 4: B and C). It is possible that the *CYP7A1* expression was also influenced by other factors such as c-jun N-terminal kinase and xenobiotic receptor (17, 18). However, since MeDCA possibly induces the export of bile acids from hepatocytes without disturbing catabolization from cholesterol to bile acids, they might effectively improve the disorder of cholesterol and bile acids. NIHS700 seemed to have properties similar to those of MeDCA, although statistically significant differences could not be observed by Dunnett's test. Therefore, further analyses about MeDCA and NIH700 are needed for effective regulation of FXR.

Since MeCA and MeDCA are methyl esters of endogenous FXR ligands, there is a question about whether these compounds are hydrolyzed and act as CA or DCA. Considering that MeDCA showed different properties in the gene expression as compared to DCA, these compounds did not seem to act as hydrolyzed forms.

The compounds screened in this study contained several non-steroidal chemicals. Marchantin A was isolated from the liverwort *Marchantia* species, as its major component (13). It shows antifungal, antimicrobial, cytotoxic, muscle-relaxing, and 5-lipoxygenase, cyclooxygenase, and calmodulin inhibitor activities [reviewed in by Asakawa et al. (19)]. The compounds with a slight structural change from marchantin A and E (i.e., marchantin B and paleatin B) did not activate FXR. It may be interesting to examine the mechanism of binding to FXR and that of the subsequent regulation of the target genes. Since these two compounds and ginkgolic acids have a much different structure from bile acids, the structural change of FXR in response to these compounds might be different from that in response to bile acids, which might result in different regulation pattern of the genes of bile acid homeostasis. In fact, marchantin A and marchantin E activated FXR diversely in each cell, although ginkgolic acids did not show FXR activation in a cell-type specific or gene-selective fashion. Bile acids function in the dietary lipid absorption and were reported to activate mitogen-activated protein kinase pathways without FXR (17, 20). The non-steroidal compounds were thought not to have these functions, although it has not been clear whether these compounds have effects other than FXR activation. Moreover, the non-steroidal compounds are not metabolized to form harmful lithocholic acid (21, 22). Therefore, it is possible that these compounds can be used for studying the pharmacology of FXR.

As described above, some compounds demonstrated properties of cell-type–specific and/or gene-selective modulators. Until now, several compounds have been found to be cell-type–specific and/or gene-selective modulators of FXR (10, 11, 16). Although the mechanism of selective FXR modulation remains to be elucidated, it was suggested that differences in coregulator recruitment play a critical role in cell-type–specific and promoter-specific regulation by other nuclear receptors (23, 24). We therefore investigated the binding capacity of FXR with receptor-interacting domains of the activator for thyroid hormone and retinoid receptors (ACTR), vitamin D–interacting protein 205 (DRIP205), glucocorticoid receptor–interacting protein (GRIP), receptor-interacting protein 140 (RIP140), and steroid receptor coactivator-1 (SRC-1) with a mammalian two-hybrid assay. However, we could not detect enough obvious differences to explain the cell-type (and/or gene) specific modulation (data not shown).

There are the other possibilities about cell-type–specific modulation, although the gene specific modulation could not be explained. First, the compounds are metabolized in cultured cells and their metabolites bind to FXR as ligands. In case that the metabolism varies with cell-type, FXR is differentially-activated. Second, the compounds are inactivated by metabolism in some cells. Third, permeability of the compounds is different according to cell-type. Since all the compounds tested were hydrophobic and separated out in culture medium at lower concentrations as compared to CDCA, the third possibility is unlikely. To reveal the mechanism of selective FXR modulation and to produce a synthetic selective modulator, farther analyses are required.

Finally, FXR has pleiotropic therapeutic potential, but a simple FXR agonist will have undesired side-effects (reviewed in refs. 25 and 26). The compounds discussed in the present paper appear to be useful for studying FXR modulation leading to selective FXR modulation for therapy.

Acknowledgments

This work was supported by a grant-in-aid (MF-16) from the Pharmaceuticals and Medical Device Agency, a

grant-in-aid for Research on Publicly Essential Drugs and Medical Devices from the Japan Health Science Foundation, and a grant-in-aid from the Ministry of Health, Labour, and Welfare of Japan.

References

1 Khorasanizadeh S, Rastinejad F. Nuclear-receptor interactions on DNA-response elements. Trends Biochem Sci. 2001;26:384–390.

2 Makishima M, Okamoto AY, Repa JJ, Tu H, Learned RM, Luk A, et al. Identification of a nuclear receptor for bile acids. Science. 1999;284:1362–1365.

3 Parks DJ, Blanchard SG, Bledsoe RK, Chandra G, Consler TG, Kliewer SA, et al. Bile acids: natural ligands for an orphan nuclear receptor. Science. 1999;284:1365–1368.

4 Wang H, Chen J, Hollister K, Sowers LC, Forman BM. Endogenous bile acids are ligands for the nuclear receptor FXR/BAR. Mol Cell. 1999;3:543–553.

5 Sinal CJ, Tohkin M, Miyata M, Ward JM, Lambert G, Gonzalez FJ. Targeted disruption of the nuclear receptor FXR/BAR impairs bile acid and lipid homeostasis. Cell. 2000;102:731–744.

6 Maloney PR, Parks DJ, Haffner CD, Fivush AM, Chandra G, Plunket KD, et al. Identification of a chemical tool for the orphan nuclear receptor FXR. J Med Chem. 2000;43:2971–2974.

7 Liu Y, Binz J, Numerick MJ, Dennis S, Luo G, Desai B, et al. Hepatoprotection by the farnesoid X receptor agonist GW4064 in rat models of intra- and extrahepatic cholestasis. J Clin Invest. 2003;112:1678–1687.

8 Zhang Y, Lee FY, Barrera G, Lee H, Vales C, Gonzalez FJ, et al. Action of the nuclear receptor FXR improves hyperglycemia and hyperlipidemia in diabetic mice. Proc Natl Acad Sci U S A. 2006;103:1006–1011.

9 Inagaki T, Moschetta A, Lee Y-K, Peng L, Zhao G, Downes M, et al. Regulation of antibacterial defense in the small intestine by the nuclear bile acid receptor. Proc Natl Acad Sci U S A. 2006;103:3920–3925.

10 Cui J, Huang L, Zhao A, Lew J-L, Yu J, Sahoo S, et al. Guggulsterone is a farnesoid X receptor antagonist in coactivator association assays but acts to enhance transcription of bile salt export pump. J Biol Chem. 2003;278:10214–10220.

11 Dussault I, Beard R, Lin M, Hollister K, Chen J, Xiao JH, et al. Identification of gene-selective modulators of the bile acid receptor FXR. J Biol Chem. 2003;278:7027–7033.

12 Suzuki T, Nishimaki-Mogami T, Kawai H, Kobayashi T, Shinozaki Y, Sato Y, et al. Screening of novel nuclear receptor agonists by a convenient reporter gene assay system using green fluorescent protein derivatives. Phytomedicine. 2006;13:401–411.

13 Asakawa Y. Chemical constituents of hepaticae. In: Herz W, Grisebach H, Kirby WG, editors. Progress in the chemistry of organic natural products, Vol. 42, Wien: Spriger; 1982, p. 1–285.

14 Asakawa Y. Biologically active terpenoids and aromatic compounds from liverworts and inedible mushroom *Cryptoporus volvatus*. In: Colegate SM, Molyneux RJ, editors. Bioactive natural products: detection, isolation, and structural determination. Florida: CRC Press; 1993, p. 319–347.

15 Mi L-Z, Devarakonda S, Harp JM, Han Q, Pellicciari R, Willson TM, et al. Structural basis for bile acid binding and activation of the nuclear receptor FXR. Mol Cell. 2003;11:1093–1100.

16 Lew JL, Zhao A, Yu J, De Pedro N, Peláez F, Wright SD, et al. The farnesoid X receptor controls gene expression in a ligand- and promoter-selective fashion. J Biol Chem. 2004;279:8856–8861.

17 Gupta S, Stravitz RT, Dent P, Hylemon PB. Down-regulation of cholesterol 7α-hydroxylase (*CYP7A1*) gene expression by bile acids in primary rat hepatocytes is mediated by the c-Jun N-terminal kinase pathway. J Biol Chem. 2001;276:15816–15822.

18 Staudinger JL, Goodwin B, Jones SA, Hawkins-Brown D, MacKenzie KI, LaTour A, et al. The nuclear receptor PXR is a lithocholic acid sensor that protects against liver toxicity. Proc Natl Acad Sci U S A. 2001;98:3369–3374.

19 Asakawa Y. Recent advances in phytochemistry of bryophytes-acetogenins, terpenoids and bis(bibenzyl)s from selected Japanese, Taiwanese, New Zealand, Argentinean and European liverworts. Phytochemistry. 2001;56:297–312.

20 Qiao L, Han SI, Fang Y, Park JS, Gupta S, Gilfor D, et al. Bile acid regulation of C/EBPβ, CREB, and c-Jun function, via the extracellular signal-regulated kinase and c-Jun NH_2-terminal kinase pathways, modulates the apoptotic response of hepatocytes. Mol Cell Biol. 2003;23:3052–3066.

21 Fischer S, Beuers U, Spengler U, Zwiebel FM, Koebe HG. Hepatic levels of bile acids in end-stage chronic cholestatic liver disease. Clin Chim Acta. 1996;251:173–186.

22 Javitt NB. Cholestasis in rats induced by taurolithocholate. Nature. 1966;210:1262–1263.

23 Kodera Y, Takeyama K, Murayama A, Suzuwa M, Masuhiro Y, Kato S. Ligand type-specific interactions of peroxisome proliferator-activated receptor gamma with transcriptional coactivators. J Biol Chem. 2000;275:33201–33204.

24 Shang Y, Brown M. Molecular determinants for the tissue specificity of SERMs. Science. 2002;295:2465–2468.

25 Modica S, Moschetta A. Nuclear bile acid receptor FXR as pharmacological target: are we there yet? FEBS Lett. 2006;580:5492–5499.

26 Cariou B, Staels B. FXR: A promising target for the metabolic syndrome? Trends Pharmacol Sci. 2007;28:236–243.

Glass-State Amorphous Salt Solids Formed by Freeze-Drying of Amines and Hydroxy Carboxylic Acids: Effect of Hydrogen-Bonding and Electrostatic Interactions

Saori KADOYA,[a] Ken-ichi IZUTSU,*[,b] Etsuo YONEMOCHI,[a] Katsuhide TERADA,[a] Chikako YOMOTA,[b] and Toru KAWANISHI[b]

[a] *Faculty of Pharmaceutical Sciences, Toho University; 2–2–1 Miyama, Funabashi, Chiba 274–8510, Japan: and* [b] *National Institute of Health Sciences; 1–18–1 Kamiyoga, Setagaya, Tokyo 158–8501, Japan.*

Received February 6, 2008; accepted April 4, 2008; published online April 7, 2008

We studied effect of molecular interactions on the physical properties of binary freeze-dried solids and frozen aqueous solutions using model chemicals containing various functional groups (amino, carboxyl, hydroxyl). Thermal analysis of frozen solutions containing alkyl diamines and hydroxy di- or tricarboxylic acids showed thermal transitions (T_g': glass transition of maximally freeze-concentrated phase) at temperatures higher than those of the individual solutes. A binary frozen solution containing 80 mM 1,3-diamino-2-hydroxypropane (single-solute $T_g' < -60$ °C) and 120 mM citric acid (single-solute T_g': −55.0 °C) made the transition at −30.8 °C. The molecular weight of the solutes had smaller effects on the transition temperatures of the frozen mixture component solutions. Lyophilization of some high T_g' mixture frozen solutions (*e.g.*, 1,3-diamino-2-hydroxypropane and citric acid) resulted in cake-structure amorphous solids with glass transition temperatures (T_g) higher than those of the individual components. Networking of intense hydrogen-bondings and electrostatic interactions between the heterogeneous molecules through the multiple functional groups was suggested to reduce the component mobility in the amorphous freeze-concentrated phase and the freeze-dried solids. Controlling the interactions should be a key to optimizing the physical properties of multi-component amorphous freeze-dried pharmaceutical formulations.

Key words freeze-drying; glass solid; thermal analysis; molecular interaction; salt

Glass-state amorphous solids are applied to pharmaceutical formulations as a way to improve dissolution of hydrophobic active ingredients (APIs) or to ensure stability of embedded biomacromolecules (*e.g.*, recombinant proteins) and drug delivery system (DDS) carriers (*e.g.*, liposome).[1—3] Freeze-drying is often a preferable method over other procedures (*e.g.*, quench-cooling of heat-melt solids) for the large-scale production of glass-state solid formulations containing thermally unstable ingredients. Dispersion of drug molecules into nonionic excipient matrices (*e.g.*, trehalose, polyvinylpyrrolidone (PVP)) is a popular way to make the non-crystalline formulations of many APIs that have intrinsic propensity for crystallization or low glass transition temperatures (T_g).[1] Insufficient miscibility with certain drug molecules and poor storage stability, however, often hinders the development of solid dispersion formulations using the nonionic matrices.

The application of salts or binary complexes is another approach to obtain stable amorphous solids.[4] For example, freeze-drying of sodium indomethacin results in an amorphous solid that has a glass transition temperature (120 °C) significantly higher than that of the free acid molecules (45 °C).[4,5] Recent studies indicated that the glass-state solids composed of excipient salts or salt-forming excipient combinations are promising as dispersion matrices.[6,7] Some pH-adjusting buffer salts (*e.g.*, monosodium citrate) form high T_g amorphous solids applicable to protein formulations.[7] Co-lyophilization of some basic amino acids (*e.g.*, L-arginine, L-lysine, L-histidine) with multivalent inorganic acids (*e.g.*, phosphoric acid) also results in the formation of protein-stabilizing glass-state solids.[6] High transition temperatures of the mixture freeze-dried solids suggest the contribution of strong intermolecular or inter-ion interactions to reducing the heterogeneous component mobility.

In contrast to the extensive studies on the physical properties and local structure of amorphous glass- or rubber-state solids composed of nonionic small molecules (*e.g.*, sucrose, sorbitol) or polymers (*e.g.*, PVP),[3] mechanisms that determine character of organic salts and/or heterogeneous components have not been well elucidated.[1,3] Recent intensive studies on ionic liquids (RTMS: room temperature molten salts) provided valuable information regarding the component ion structures, participating interactions, and the physical properties of the microscopically unordered non-crystalline salt systems.[8] Some earlier studies indicated feasibility to control the physical property of the amorphous salt solids by optimizing the component structure (*e.g.*, ion radius in indomethacin alkali metal salts)[4] and their compositions that determine the intermolecular and/or inter-ion interactions.

The purpose of this study was to elucidate the contribution of functional groups and the size of consisting molecules to the physical properties of multi-component frozen aqueous solutions and their freeze-dried solids. Thermal analysis of various combinations of model chemicals containing amino, carboxyl, and/or hydroxyl groups was performed to obtain the thermal transition temperatures (T_g, T_g': glass transition temperature of maximally freeze-concentrated phase) and propensity for crystallization in the frozen solutions and freeze-dried solids. Mid- and near-infrared analysis was performed to elucidate the molecular interaction in the freeze-dried solids. We also discuss the application of the amorphous mixture solids to pharmaceutical formulations.

* To whom correspondence should be addressed. e-mail: izutsu@nihs.go.jp

Experimental

Materials 1,3-Diaminopropane was purchased from Kanto Kagaku Kogyo Co. (Tokyo, Japan). 1,3-Diamino-2-hydroxypropane was the product of Sigma-Aldrich Inc. (St. Louis, MO, U.S.A.). Tricarballylic acid was obtained from Alfa Aesar GmbH & Co. KG (Karlsruhe, Germany). DL-Malic acid, D-(+)-malic acid, glycolic acid, L-(+)-tartaric acid, glutaric acid, adipic acid, DL-lactic acid (2-hydroxypropanoic acid), 1-aminopropane (propylamine), 1,4-diaminobutane, 1,6-diaminohexane, 1,8-diaminooctane, and other reagents were of analytical grade obtained from Wako Pure Chemical Industries Co. (Osaka, Japan).

Thermal Analysis Thermal analysis of frozen solutions and freeze-dried solids was conducted with a differential scanning calorimeter (DSC Q-10, TA Instruments, New Castle, DE, U.S.A.) with Universal Analysis 2000 software (TA Instruments). An aliquot (10 μl) of aqueous solution in an aluminum cell was cooled to -70 °C at 10 °C/min and then scanned at 5 °C/min. Freeze-dried solids (1—2 mg) in hermetic aluminum cells were scanned from -30 °C at 5 °C/min under nitrogen flow. Physical mixtures containing 1,3-diamino-2-hydroxypropane and citric acid (1.5—2.5 mg) in aluminum cells were melted at 165 °C for 3 min and then cooled rapidly by immersion in liquid nitrogen to prepare quench-cooled melt solids. The cells were transferred to the furnace of the calorimeter at 15 °C and then scanned from -50 °C at 5 °C/min to obtain the glass transition temperatures. Glass transition temperatures were determined as the maximum inflection point of the discontinuities in the heat flow curves.

Freeze-Drying A freeze-drier (Freezone-6, Labconco, Kansas City, MO, U.S.A.) equipped with temperature-controlling trays was used for lyophilization. Aqueous solutions containing the solutes (total 200 mM, 300 μl) in flat-bottom glass vials (13 mm diameter) were placed on the shelf of the freeze-drier at room temperature. The shelf was cooled to -40 °C at 0.5 °C/min and then maintained at that temperature for 2 h before drying. The frozen solutions were dried under vacuum (21 mTorr) maintaining the shelf temperature at -40 °C for 15 h, -30 °C for 6 h, and 35 °C for 6 h. The shelf was heated at 0.2 °C/min between the drying steps. The vials were closed with rubber stoppers under the vacuum. Solids for near-infrared analysis were prepared by freeze-drying the aqueous solutions (1 ml) in larger vials (18 mm diameter).

Mid- and Near-Infrared Spectroscopy (IR, NIR) An FT-IR spectrophotometer (MB104, ABB Bomen, Quebec, Canada) and GRAMS/32 software (Galactic Ind. Co., Salem, NH, U.S.A.) were used to obtain mid-infrared spectra of the solids (approx. 1 mg sample solid) in a pressed potassium bromide disk (approx. 250 mg). Transition spectra of the sample disks were obtained at 4 cm^{-1} resolution in 128 scans. Near-infrared spectroscopy was performed by using a Bruker MPA system with a diffuse-reflectance integrating-sphere probe (PbS detector) and OPUS software (Ettlingen, Germany). Near-infrared light was directed upward from the bottom of the glass vials containing freeze-dried solids to obtain the reflected signal over a range of 4000—12000 cm^{-1} with a resolution of 4 cm^{-1} in 128 scans.

Powder X-Ray Diffraction (XRD) and Residual Water Content Measurement The powder X-ray diffraction patterns were measured at room temperature with a Rint-Altima diffractometer (Rigaku, Tokyo, Japan) with Cu$K\alpha$ radiation at 40 kV/40 mA. The samples were scanned in the area of $5° < 2\theta < 35°$ at an angle speed of 5°/min. An AQV-6 volumetric titrator (Hiranuma Sangyo, Ibaraki, Japan) was used to determine the amount of water in the freeze-dried solids suspended in dehydrated methanol by the Karl–Fischer method.

Results

Figure 1 shows thermograms of frozen aqueous solutions containing a carboxylic acid and an amide (200 mM). The structure of the chemicals used in this study and their physical properties in the frozen solutions obtained by thermal analysis are summarized in Table 1. Some solutes showed intrinsic propensities to crystallize in the freeze-concentrated phases. An endotherm (-15.8 °C) in a frozen malonic acid solution suggested melting of the eutectic crystal. The exotherm (-53.1 °C) and endotherm (-19.3 °C) peaks

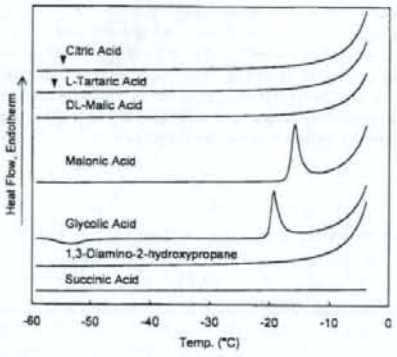

Fig. 1. Thermograms of Frozen Solutions Containing a Carboxylic Acid or an Amine (200 mM)

Aliquots (10 μl) of solutions in hermetic aluminum cells were scanned from -70 °C at 5 °C/min. Arrowheads denote the glass transition of maximally freeze-concentrated solutes (T_g').

Table 1. Structure and Thermal Property of Carboxylic Acids and Amines in Frozen Aqueous Solutions Obtained by Thermal Analysis

	MW	Functional groups			Property in frozen solutions	
		COOH	OH	NH_2	Crystallinity	Thermogram
Acetic acid	60.1	1	0	0	Crystallized	Endotherm
Glycolic acid	76.1	1	1	0	Crystallized	Exotherm/endotherm
DL-Lactic acid	90.1	1	1	0	Amorphous	$T_g' < -60$ °C
Malonic acid	104.1	2	0	0	Crystallized	Endotherm
Succinic acid	118.1	2	0	0	Crystallized	Flat
Glutaric acid	132.1	2	0	0	Crystallized	Flat
Adipic acid	146.1	2	0	0	Crystallized	Exotherm
Pimeric acid	160.2	2	0	0	Crystallized	Flat
L-Malic acid	134.1	2	1	0	Amorphous	$T_g' < -60$ °C
L-Tartaric acid	150.1	2	2	0	Amorphous	T_g': -57.1 °C
Tricarballylic acid	176.1	3	0	0	Amorphous	T_g': -52.1 °C
Citric acid	192.1	3	1	0	Amorphous	T_g': -55.1 °C
1-Aminopropane	59.1	0	0	1	Crystallized	Endotherm
3-Amino-1-propanol	75.1	0	1	1	Amorphous	$T_g' < -60$ °C
1,3-Diaminopropane	74.1	0	0	2	Amorphous	$T_g' < -60$ °C
1,4-Diaminobutane	88.2	0	0	2	Crystallized	Endotherm
1,6-Diaminohexane	116.2	0	0	2	Crystallized	Endotherm
1,8-Diaminooctane	144.3	0	0	2	Crystallized	Flat
1,3-Diamino-2-hydroxypropane	90.1	0	1	2	Amorphous	$T_g' < -60$ °C

observed in a heating scan of a frozen glycolic acid solution indicated eutectic crystallization and subsequent melting, respectively. The flat thermogram of a frozen succinic acid solution up to the ice-melting temperature suggested crystallized solutes. Some of these frozen solutions showed an exotherm that indicated eutectic crystallization in the cooling process before the thermal scan (data not shown). L-Tartaric acid and citric acid remained amorphous in the freeze-concentrated phase, presenting glass transition of the maximally freeze-concentrated solute phase (T_g') at $-55.1\,°C$ and $-57.1\,°C$, respectively.[7] The absence of particular thermal transitions and the gradual shift of the thermogram in some other single-solute frozen solutions (*e.g.*, DL-malic acid, 1,3-diamino-2-hydroxypropane) suggested that T_g' transition of the amorphous concentrated phase occurred at temperatures below the measurement temperature range ($<-60\,°C$).

Figures 2 and 3 show T_g' of frozen binary solutions containing various diamines and L-tartaric acid or citric acid. Most of the solute combinations showed a bell-shaped profile of T_g' that depended largely on the number of functional groups in the amines. Frozen mixture solutions containing amines and citric acid showed the T_g' peaks at lower acid molar ratios than in the combination with L-tartaric acid. Transition temperatures (T_g') of frozen solutions containing the acids and various diamines were significantly higher than those of the mixtures with monoamines (*e.g.*, 1-aminopropane). Slightly higher transition temperatures of the frozen solutions containing citric acid and 1,8-diaminooctane compared to those with smaller alkyldiamines (*e.g.*, 1,3-diaminopropane) indicated a relatively small effect of the component molecular size on the T_g' of the mixture phases. Introduction of hydroxyl groups to a diamine (*e.g.*, 1,3-diaminopropane to 1,3-diamino-2-hydroxypropane) raised the T_g' of the frozen mixture solutions to some extent. Mixing with L-tartaric acid or citric acid prevented crystallization of some amines (*e.g.*, 1,4-diaminobutane) in the frozen solutions. In contrast, some frozen mixture solutions showed thermal peaks that suggested crystallization of the salts. For example, a frozen solution containing 60 mM diaminooctane and 140 mM L-tartaric acid showed a T_g' ($-32.7\,°C$) and a eutectic crystallization exotherm peak ($-19.9\,°C$) in a thermal scan (data not shown).

Mixing of 1,3-diamino-2-hydroxypropane and some carboxylic acids (*e.g.*, succinic acid) also induced a significant upward shift of the T_g' (Fig. 4). The transition temperatures depended largely on the compositions of the carboxyl and hydroxyl groups in the acids. Most of the frozen mixture solutions showed the highest T_g' at the solute concentration ratios relatively rich in carboxylic acid. Alkyl chain length of the dicarboxylic acids gave limited effects on the T_g' of the mixture frozen solutions. DL-Malic acid and D-malic acid presented virtually identical T_g' profiles of the mixture frozen solutions. Mixing with 1,3-diamino-2-hydroxypropane prevented crystallization of some dicarboxylic acids (*e.g.*, malonic acid, pimeric acid) in the frozen solutions (data not shown). High T_g' of the frozen solutions containing 1,3-diamino-2-hydroxypropane and the hydroxy carboxylic acids (DL-malic acid, L-tartaric acid, citric acid) indicated a large effect of the hydroxyl group in reducing the component mobility in the freeze-concentrated phase. Frozen solutions containing 1,3-diamino-2-hydroxypropane and acetic acid or glycolic acid showed a gradual shift of the thermograms that suggested an amorphous mixture freeze-concentrated phase with T_g' below the measurement temperature range ($<-60\,°C$) (data not shown). The absence of apparent thermal transitions in frozen solutions containing some dicarboxylic

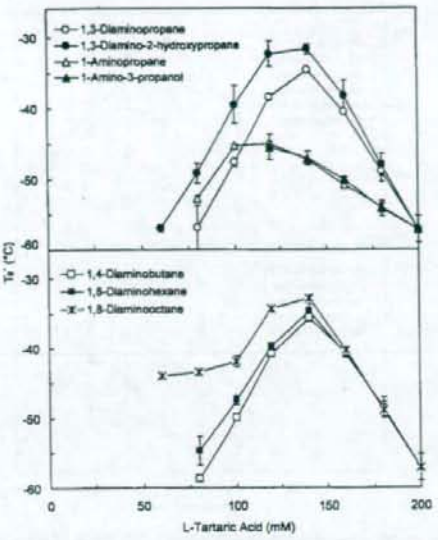

Fig. 2. Glass Transition Temperatures of the Maximally Freeze-Concentrated Phase (T_g') of Frozen Aqueous Solutions Containing L-Tartaric Acid and Various Amines

Frozen solutions (10 μl, 200 mM total) were scanned from −70 °C at 5 °C/min ($n=3$).

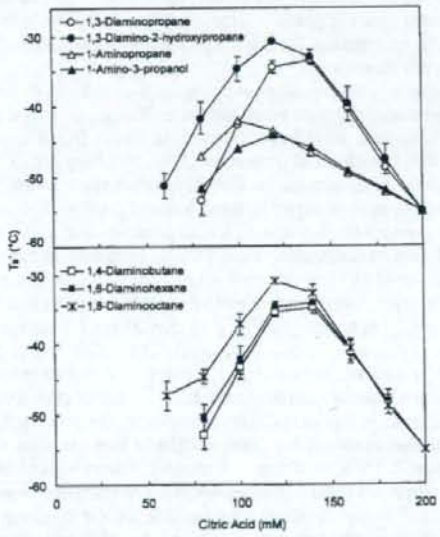

Fig. 3. Glass Transition Temperatures of the Maximally Freeze-Concentrated Phase (T_g') of Frozen Aqueous Solutions Containing Citric Acid and Various Amines

Frozen solutions (10 μl, 200 mM total) were scanned from −70 °C at 5 °C/min (average±S.D., $n=3$).

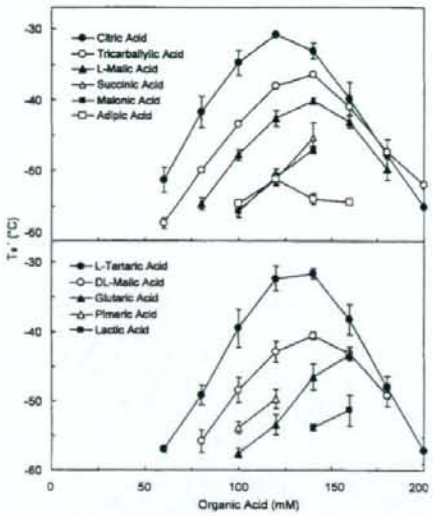

Fig. 4. Glass Transition Temperatures of the Maximally Freeze-Concentrated Phase (T_g') of Frozen Aqueous Solutions Containing 1,3-Diamino-2-hydroxypropane and Various Carboxylic Acids

Frozen solutions (10 μl, 200 mM total) were scanned from −70 °C at 5 °C/min (average±S.D., $n=3$).

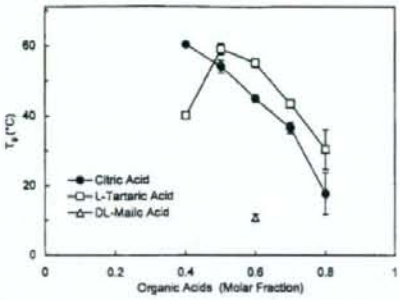

Fig. 5. Glass Transition Temperatures (T_g) of Freeze-Dried Solids Containing 1,3-Diamino-2-hydroxypropane and Organic Acids

The solids (1—2 mg) obtained by freeze-drying of aqueous solutions (200 mM total) were scanned from −30 °C at 5 °C/min (average±S.D., $n=3$).

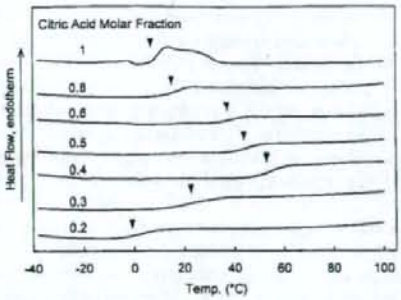

Fig. 6. Thermograms of Quench-Cooled Melt Mixture Solids Containing 1,3-Diamino-2-hydroxypropane and Citric Acid

The solids (1.5—2.5 mg) obtained by immersion of the heat-melt into liquid nitrogen were scanned from −30 °C at 5 °C/min.

acids (*e.g.*, succinic acid) and diamines (*e.g.*, diaminopropane) also suggested a large contribution of the hydroxyl groups to forming the high T_g' freeze-concentrated phase (data not shown).

Aqueous solutions containing 1,3-diamino-2-hydroxypropane and a hydroxy carboxylic acid (*e.g.*, DL-malic acid, L-tartaric acid, citric acid, 200 mM total) were freeze-dried to examine the physical properties of the resulting solids. The primary drying process at a shelf temperature (−40 °C) induced physical collapse in some lower T_g' (<−40 °C) samples, presumably because of the large molecular mobility of the freeze-concentrated phase.[9] Other frozen solutions were freeze-dried as cake-structure solids. Thermal analysis of the freeze-dried cake-structure mixture solids showed glass transitions (T_g) as high as 60.2 °C (Fig. 5, 120 mM 1,3-diamino-2-hydroxypropane, 80 mM citric acid). The solids freeze-dried from solutions containing 1,3-diamino-2-hydroxypropane and citric acid or L-tartaric acid at a 1 : 1 molar ratio showed amorphous components (halo patterns in the powder X-ray diffraction analysis) that have relatively high residual water (approx. 7—9%, w/w, data not shown). Amorphous solids of pure citric acid and 1,3-diamino-2-hydroxypropane were not available in the freeze-drying because of the physical collapse and crystallization that occurred during the process.

Quench-cooled heat-melt mixture solids containing 1,3-diamino-2-hydroxypropane and citric acid also showed a mixing-induced upward shift of the glass transition temperatures (Fig. 6). The highest transition temperature (54.5 °C) of the 0.4 citric acid molar fraction was slightly lower than that of the freeze-dried solid. Citric acid showed the glass transition of the quench-cooled solid at 9.5 °C.[10—12] The T_g of amorphous 1,3-diamino-2-hydroxypropane was not available using this method, and its low melting temperature (approx. 40—44 °C) strongly suggested a T_g below 0 °C (data not shown).

Mid-infrared analysis (FT-IR, KBr tablet transmission) of the amorphous mixture solids (0.5 citric acid molar fraction) prepared by freeze-drying and quench-cooling showed broad absorption bands (Fig. 7). Some relatively weak bands (*e.g.*, 1568 cm^{-1}) in the quench-cooled solid suggested evaporation of 1,3-diamino-2-hydroxypropane in the heating process. Non-destructive diffuse-reflection near-infrared (NIR) analysis of the freeze-dried mixture solids also showed broad bands typical for the amorphous solids (Fig. 8). Absence of some bands (*e.g.* N–H stretch 1st overtone of amino group at 6519 cm^{-1})[13] in the co-lyophilized solid (0.5 citric acid molar fraction) strongly suggested the interaction between the heterogeneous components that altered environment around the functional groups.

Discussion

Mixing of the alkyl diamines and hydroxy di- or tri-carboxylic acids induced high transition temperature amorphous concentrated phases in frozen aqueous solutions.[14] Some of the solute combinations formed cake-structure glass-state amorphous solids during freeze-drying. The high transition temperatures (T_g' and T_g) should allow faster drying processes at higher product temperature without physical collapse or shrinking of the solids.[9,15—17] Primary drying should

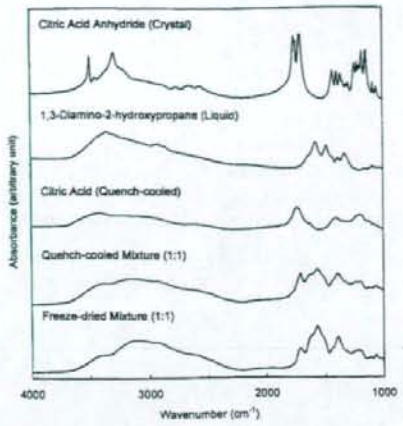

Fig. 7. FT-IR Spectra of Solids Containing 1,3-Diamino-2-hydroxypropane and Citric Acid

The mixture solids were obtained by quench-cooling of a melt (1 : 1 molar ratio, 165 °C, 3 min) or by freeze-drying of a solution (100 mM each).

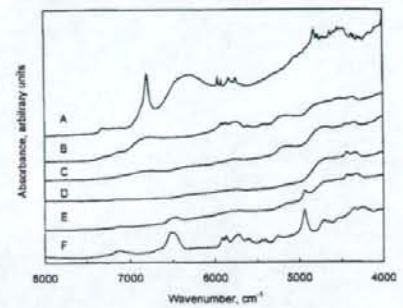

Fig. 8. Diffuse-Reflection Near-Infrared Spectra of Samples Containing 1,3-Diamino-2-hydroxypropane and Citric Acid

Each line denotes spectrum of anhydrous citric acid crystal powder (A), quench-cooled anhydrous citric acid melt (B), 1,3-diamino-2-hydroxypropane liquid (F), and solid lyophilized at the citric acid molar fraction of 0.3 (C), 0.5 (D), 0.7(E).

be conducted below the collapse temperature of the system (T_c), usually adjacent to and/or several degrees higher than the T_g', to obtain the pharmaceutically acceptable cake-structure solids. The primary drying is usually conducted at above −40 °C to accomplish ice sublimation on a practical timescale. Exposure of the partially dried solids above their glass transition temperature in the secondary drying process may shrink the cakes.

The bell-shaped profiles of the transition temperatures (T_g', T_g) depending on the component concentration ratio suggested strong attractive interaction between the components in the amorphous freeze-concentrated phase and the freeze-dried solids. Ideal mixing of nonionic molecules without particular attractive or repulsive interactions resulted in their glass transition at temperatures between those of the individual components, following the Gordon–Taylor equation.[11,18–20] It is also empirically known that frozen solutions containing the nonionic solute combinations have their thermal transition at temperatures (T_g') between those of individual solutes.[21,22] Significant upward deviation of the transition temperatures from those in the equation indicated the strong attractive interaction between the heterogeneous components. The mixing-induced transition temperature shift is also described as increasing "effective molecular weights" because many nonionic molecules (*e.g.*, polyols, saccharides) have the thermal transitions of the amorphous solids (T_g) or frozen solutions (T_g') at higher temperatures upon increasing the molecular weights.[23,24]

Networking of intense electrostatic interactions and hydrogen-bondings between the multiple functional groups should be a primary mechanism that raises the transition temperatures of the freeze-concentrated solute mixture phase and the freeze-dried solids.[4,6,25] The alkyl diamines and hydroxy di- or tri-carboxylic acids form ion pairs in aqueous solutions, and possibly in the freeze-concentrated phase. Some protonated polyamines selectively and strongly interact with particular dicarboxylates in aqueous solutions.[26] The ammonium carbohydrate ion pairs form multiple hydrogen-bonding in some non-polar solvents.[27,28] Continuous network of electrostatic interactions and hydrogen-bonding make the salt crystals popular supermolecular building blocks.[29] The differently protonated carboxyl and carboxylate groups also form an intermolecular hydrogen-bonding anion network.[30] It is plausible that the multi-component interactions contribute to the high transition temperature of the amorphous freeze-concentrated phase (T_g') and the freeze-dried solids (T_g). The eutectic crystallization observed in some high T_g' frozen solutions (*e.g.*, 60 mM diaminooctane and 140 mM L-tartaric acid) suggested effective interactions that induce the spatial ordering of the salt components above the transition temperature. Introduction of the hydroxyl groups to the components should provide additional hydrogen bonding in the amorphous phases. The limited effect of the component size on the transition temperatures also supported the significance of the interaction networks in determining physical properties.[23] Various factors, including the component structures, molar ratios, and water contents should alter the contribution of hydrogen-bonding and electrostatic (*e.g.*, ion–ion, ion–dipole, dipole–dipole) interactions in the amorphous phases. Further information on the interactions remains to be elucidated by other analytical methods (*e.g.*, solid-state NMR).

Recent studies on ionic liquids (RTMS: room temperature molten salt) also indicated the significant contribution of intermolecular (inter-ion) interactions to determining the physical properties of the locally disordered liquid or amorphous solid systems.[31,32] Factors that provide weak interaction between the molecules and/or ions (*e.g.*, size, charge distribution, functional groups) should induce low glass transition temperatures and low viscosities relevant to ionic liquids.[8] In contrast, glass-state solids would be designed by introducing strong interactions between the heterogeneous components.

The glass-state multi-component amorphous solids should be applicable in pharmaceutical formulations in several ways. Certain excipient mixture glass solids would become molecular dispersion matrixes that enable rapid dissolution of active ingredients or stabilization of biomacromolecules.[6] Some basic amino acids (*e.g.*, L-arginine) would be practical choices to form the glass-state mixture solids applicable in pharmaceutical formulations. The weakly acidic to alkaline pH of the high T_g mixtures and their re-hydrated solutions

Biochemistry **2008,** *47,* 10132–10154

Glycosylation Analysis of IgLON Family Proteins in Rat Brain by Liquid Chromatography and Multiple-Stage Mass Spectrometry†

Satsuki Itoh,‡ Akiko Hachisuka,‡ Nana Kawasaki,*,‡,§ Noritaka Hashii,‡ Reiko Teshima,‡ Takao Hayakawa,∥ Toru Kawanishi,‡ and Teruhide Yamaguchi‡

Division of Biological Chemistry and Biologicals, National Institute of Health Sciences, 1-18-1, Kamiyoga, Setagaya-ku, Tokyo 158-8501, Japan, Core Research for Evolutional Science and Technology of Japan Science and Technology Agency, Kawaguchi Center Building, 4-1-8 Hon-cho, Kawaguchi, Saitama 332-0012, Japan, and Pharmaceutical Research and Technology Institute, Kinki University, 3-4-1 Kowakae, Higashi-Osaka 577-8502, Japan

Received May 23, 2008; Revised Manuscript Received July 17, 2008

ABSTRACT: IgLON family proteins, including limbic-associated membrane protein (LAMP), opioid-binding cell adhesion molecule (OBCAM), neurotrimin, and Kilon, are immunoglobulin (Ig) superfamily cell adhesion molecules. These molecules are composed of three Ig domains and a glycosylphosphatidylinositol (GPI) anchor and contain six or seven potential N-glycosylation sites. Although their glycosylations are supposed to be associated with the development of the central nervous system like other Ig superfamily proteins, they are still unknown because of difficulty in isolating individual proteins with a high degree of homology in performing carbohydrate analysis. In this study, we conducted simultaneous site-specific glycosylation analysis of rat brain IgLON proteins by liquid chromatography and multiple-stage mass spectrometry (LC−MS^n). The rat brain GPI-linked proteins were enriched and separated by sodium dodecyl sulfate−polyacrylamide gel electrophoresis. The four proteins were extracted from the gel, and subjected to LC−MS^n after proteinase digestions. A set of glycopeptide MS data, including the mass spectrum, the mass spectrum in the selected ion monitoring mode, and the product ion spectra, was selected from all data based on carbohydrate-related ions in the MS/MS spectrum. The peptide portion and the carbohydrate structure were identified on the basis of peptide-related ion and carbohydrate-related ions, and the accurate mass. The site-specific glycosylations of four proteins were elucidated as follows. *N*-Glycans near the N-terminal were disialic acid-conjugated complex- and hybrid-type oligosaccharides. The first Ig domains were occupied by Man-5-9. Diverse oligosaccharides, including Lewis a/x-modified glycans, a brain-specific glycan known as BA-2, and Man-5, were found to be attached to the third Ig domain. Three common structures of glycans were found in the GPI moiety of LAMP, OBCAM, and neurotrimin.

Cell adhesion molecules on cell surfaces are involved in several biological events, such as cell−cell interaction, signaling, and cellular traffic. In the central nervous system, cell adhesion molecules are associated with the differentiation and migration of neurons, and neurite outgrowth. The immunoglobulin (Ig) superfamily, which contains one or more Ig-like domains, is known as one of the cell adhesion molecule families in the central nervous system (*1*). The Ig superfamily includes various proteins, such as P0, Thy-1, myelin-associated glycoprotein (MAG), neural cell adhesion molecule (NCAM), L1, contactin, and IgLON family proteins. Glycosylation of the Ig superfamily proteins is known to be involved in cell−cell interactions (*2*−*4*). Polysialylated glycans in the fifth domain of NCAM are thought to inhibit the interaction of NCAM with other molecules and to promote neural plasticity through a repulsive interaction (*5*, *6*). The HNK-1 epitope in the third and fifth domains of NCAM is known to mediate molecular recognition in the nervous system (*7*).

The IgLON superfamily includes the limbic-associated membrane protein (LAMP),[1] the opioid-binding cell adhesion molecule (OBCAM), neurotrimin, and Kilon (*8*−*14*), and

† This work was supported in part by a Grant-in-Aid from the Ministry of Health and Labor and Welfare, and Core Research for Evolutional Science and Technology Program (CREST) of the Japan Science and Technology Agency (JST).

* To whom correspondence should be addressed: Division of Biological Chemistry and Biologicals, National Institute of Health Sciences, 1-18-1, Kamiyoga, Setagaya-ku, Tokyo 158-8501, Japan. Telephone: +81-3-3700-9074. Fax: +81-3-3707-6950. E-mail: nana@nihs.go.jp.

‡ National Institute of Health Sciences.

§ Core Research for Evolutional Science and Technology of Japan Science and Technology Agency.

∥ Kinki University.

[1] Abbreviations: LC, liquid chromatography; MS, mass spectrometry; MS^n, multiple-stage mass spectrometry; LAMP, limbic-associated membrane protein; OBCAM, opioid-binding cell adhesion molecule; GlcNAc, *N*-acetylglucosamine; GPI, glycosylphosphatidylinositol; PI-PLC, phosphatidylinositol-specific phospholipase C; PNGase F, peptide *N*-glycosidase F; IT-MS, ion trap mass spectrometer; FT ICR-MS, Fourier transform ion cyclotron resonance mass spectrometer; GCC, graphitized carbon column; TIC, total ion chromatogram; CID, collision-induced dissociation; SIM, selected ion monitoring; dHex, deoxyhexose; Hex, hexose; HexNAc, *N*-acetylhexosamine; Fuc, fucose; Man, mannose; Gal, galactose; GlcNAc, *N*-acetylglucosamine; GlcN, glucosamine; NeuAc, *N*-acetylneuraminic acid; $EtNH_2$, ethanolamine; Ino, inositol; BA-2, brain-specific sugar chain, GlcNAcβ1−2Manα1−6(GlcNAcβ1−4)(GlcNAcβ1−2Manα1−3)Manβ1−4GlcNAcβ1−4(Fucα1−6)GlcNAc; SDS−PAGE, sodium dodecyl sulfate−polyacrylamide gel electrophoresis.

10.1021/bi8009778 CCC: $40.75
Published on Web 08/26/2008

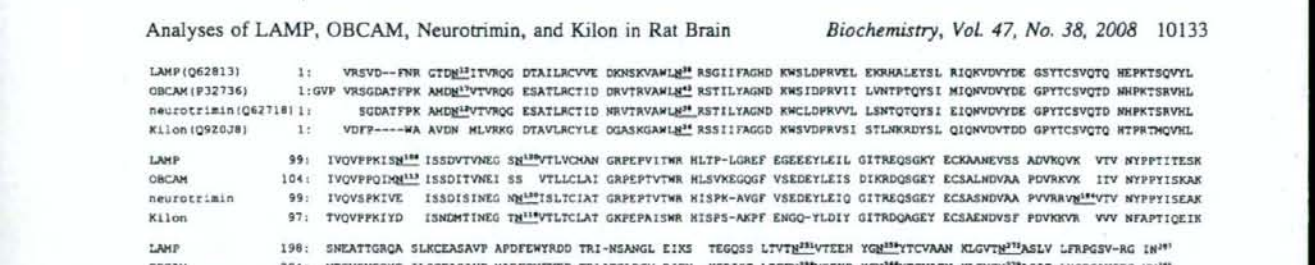

FIGURE 1: Amino acid sequence and potential N-glycosylation sites (in bold) of IgLON family proteins. Their accession numbers in Swiss-prot database are shown in parentheses after their names. The C-terminal amino acids in the proteins are predicted GPI attachment sites.

these proteins are distributed differently in the central nervous system during the development of neurons in a brain (*11*, *13*−*18*). The IgLON family proteins consist of three Ig domains, the third of which is attached to a glycosylphosphatidylinositol (GPI) anchor. Each of the IgLON family proteins includes six or seven consensus N-glycosylation sites (Figure 1), and the glycosylation is presumed to play essential roles in the neural circuit formation like other Ig superfamily proteins (*2*−*4*). However, since the high degree of homology of their amino acid sequences makes it difficult to isolate the individual proteins of this family to perform carbohydrate analysis, their glycosylation features are still unknown with the exception of a linkage of *N*-glycans in OBCAM and Kilon and of high mannose-type and hybrid-type oligosaccharides in LAMP (*9*, *18*, *19*).

Recently, liquid chromatography and mass spectrometry (LC−MS) and liquid chromatography and multiple-stage mass spectrometry (LC−MS^n) have been widely applied to the site-specific glycosylation analysis of a glycoprotein (*20*−*24*). Generally, a tryptic digest of an isolated glycoprotein is separated with a reversed-phase or normal-phase column, and the separated glycopeptides are directly subjected to MS and MS^n (*25*−*27*). The site-specific glycosylation is deduced from the mass spectra of the glycopeptides, and the sequences of both the peptide and carbohydrate portions are deduced from the fragment ions in the MS^n spectra. Using this technique, we previously performed a site-specific glycosylation analysis of rat brain Thy-1, which contains three N-glycosylation sites and a GPI anchor (*28*). GPI-anchored proteins enriched via phase partitioning with Triton X-114 and PIPLC digestion were separated by SDS−PAGE, and the Thy-1 protein extracted from the gel was digested with trypsin or endoproteinase Asp-N. The Thy-1 glycopeptides were separated and analyzed by using a liquid chromatography and ion trap mass spectrometer (IT-MS) equipped with a C18 column. The peptide portions of glycopeptides were identified on the basis of the *m*/*z* values of the peptide-related ions and the b- and y-ions that arose from the peptide backbone. The carbohydrate structures at each glycosylation site and in the GPI moiety were successfully determined from fragment ions in the MS/MS spectra. This result suggests that LC−MS^n can be effectively utilized for site-specific glycosylation analysis of each glycoprotein in the mixture of several glycoproteins simultaneously.

In this study, we conducted site-specific glycosylation analyses of rat LAMP, OBCAM, neurotrimin, and Kilon using LC−MS^n. The GPI-linked proteins in the rat brains were separated by SDS−PAGE, and the IgLON family proteins were extracted from a gel band (45−70 kDa). The mixture of proteins was digested with proteinases, and the site-specific glycosylation analysis of the four proteins was performed by using an ion trap-Fourier transform ion cyclotron resonance mass spectrometer (IT-MS-FT ICR-MS), which is capable of acquiring the accurate mass as well as the MS^n spectra. We successfully elucidated the site-specific glycosylation and the structure of the GPI moieties of LAMP, OBCAM, neurotrimin, and Kilon. This is the first report of the simultaneous site-specific glycosylation analysis of four similar glycoproteins.

EXPERIMENTAL PROCEDURES

Materials. The rat brains (Wister, male, 3 weeks old) were purchased from Nippon SLC (Hamamatsu, Japan). Phosphatidylinositol-specific phospholipase C (PIPLC) from *Bacillus cereus* was obtained from Molecular Probes (Eugene, OR). Trypsin-Gold was purchased from Promega (Madison, WI). PNGase F and endoproteinase Glu-C were purchased from Roche Diagnostics (Mannheim, Germany). SimplyBlue SafeStain was obtained from Invitrogen (Carlsbad, CA). All other chemicals were of the highest available purity.

SDS−PAGE of Enriched Lipid-Free GPI-Linked Proteins. Lipid-free GPI-linked proteins were enriched from rat brain as reported previously (*28*, *29*). Briefly, the homogenate of two rat brains (total wet weight of 1.4 g) was defatted and solubilized with 2% Triton X-114 at 4 °C overnight (*29*, *30*). After centrifugation, the supernatant was subjected to Triton X-114 phase partitioning at 37 °C. Cold acetone was added to the detergent phase containing solubilized membrane proteins, and the resulting precipitate was digested with PIPLC. After the PIPLC digest mixture had been subjected to Triton X-114 phase partitioning, lipid-free GPI-linked proteins in the aqueous phase were precipitated via addition of cold acetone. These proteins were separated by SDS−PAGE (12.5%) (brain wet weight of 50 mg/lane) after carboxyamidomethylation (*31*) and detected after being stained with Coomassie Brilliant Blue G-250 using SimplyBlue SafeStain.

Protein Identification. Gel-separated proteins were extracted after in-gel trypsin digestion as previously reported (*32*) and subjected to LC−MS/MS with a Paradigm MS4 HPLC system (Michrom BioResources, Inc., Auburn, CA) consisting of pump A with 0.1% formic acid and 2% acetonitrile and pump B with 0.1% formic acid and 90% acetonitrile. Peptides were separated with a Magic C18 column (50 mm × 0.2 mm, 3 μm; Michrom BioResources Inc.) with a linear gradient from 5 to 65% of pump B over